PHYSICAL REVIEW D VOLUME 15, NUMBER 1 1 JANUARY 1977

Neutron spectra at 0° from proton-proton collisions between 647 and 805 MeV*

G. Glass, Mahavir Jain, M. L. Evans,† J. C. Hiebert, and L. C. Northcliffe
Texas A & M University, College Station, Texas 77843

B. E. Bonner and J. E. Simmons
Los Alamos Scientific Laboratory, Los Alamos, New Mexico 87545

C. Bjork‡ and P. Riley
University of Texas, Austin, Texas 78712

C. Cassapakis§
University of New Mexico, Albuquerque, New Mexico 87106
(Received 23 August 1976)

Momentum spectra of neutrons at 0° from the process $pp \rightarrow np\pi^+$ have been measured at 647, 771, and 805 MeV. Absolute cross sections $d^2\sigma/d\Omega dp$ and $d\sigma/d\Omega^*$ are given for all three energies. A phenomenological calculation using only S- and P-wave πN phase shifts and an NN final-state interaction appears to account for the shapes and magnitudes of the spectra quite well. Comparison with the process $np \rightarrow pX$ indicates a non-negligible contribution from nonresonant amplitudes.

I. INTRODUCTION

The nucleon-nucleon (NN) interaction, although not elementary from a particle-physics point of view, is fundamental and extremely important to nuclear physics. The determination of an unambiguous and accurate scattering matrix for NN collisions must perforce overcome the obstacles presented by the effects of pion production. Therefore, insights to be gained from a study of pion production in NN collisions would contribute toward a better understanding of the NN interaction, as well as furthering our knowledge of the πN interaction.

In the present experiment momentum spectra have been measured for 0° neutrons from the reaction

$$pp \rightarrow np\pi^+ \tag{1}$$

for $T_p = 647$, 771, and 805 MeV. The quantity of accumulated data and the momentum resolution (~1%) are sufficient to provide ~5% statistical precision in 20-MeV/c bins, which until now has not been available in this kinematic region and in this incident energy range. These data allow for critical tests of theories on pion production at these energies, and since at each neutron momentum, P_n, the value of the πp invariant mass, $M_{\pi p}$, is uniquely determined, the cross section $d^2\sigma/dpd\Omega$ directly reflects the effects of the $\Delta(1232)$ resonance. This latter feature helps one to deduce the contribution from nonresonant amplitudes for which the πN isospin equals $\frac{1}{2}$. Although extensive studies both theoretically[1-9] and experimentally[10-24] have been conducted, no single phenomenological model has yet been shown to quantitatively explain the results in this energy region. However, we make use of a modified version of a code developed by Stephenson, Gibbs, and Gibson[5] (referred to as SGG) and find that by appropriate adjustment of four parameters rather good fits are obtained at all three energies investigated here. Some further discussion of the parametrization of these fits is given in Sec. V. Other treatments have been quite successful in other energy regions. The peripheral model with absorption[9] does fairly well from 1.3 to 9 GeV, but the influence of many baryon resonances [especially the $\Delta(1232)$] in the region from 800 to 1300 MeV makes necessary a phenomenological treatment such as the one-pion-exchange (OPE) model.[2] Below 650 MeV, where the only significant resonant contribution comes from the $\Delta(1232)$, and where the NN final-state interaction (FSI) plays an important role, Mandelstam's treatment[1] has been successful. However, in the region between 650 and 800 MeV neither the low-energy[1,4] nor the higher-energy[2,3] models are valid, which makes the measurements presented here interesting especially in view of the potentially viable treatment of SGG.[5]

Previous measurements of neutron spectra from the process in Eq. (1) have been made by Guzhavin *et al.*[13] and Bugg *et al.*[14] from bubble-chamber measurements of the proton and pion momenta. However, since the number of events was small (430 and 1414, respectively) their spectra necessarily had to include integration over the neutron solid angle, $\Delta\Omega_n = 4\pi$. More detailed information in this energy region is furnished by recent experiments at the Clinton P. Anderson Meson

Physics Facility (LAMPF). Pratt *et al.*[21] have measured neutron spectra at 0°, 14°, and 27° for $pp \to np\pi^+$ at 800 MeV by a time-of-flight (TOF) technique, and for the same process also at 800 MeV Hudomalj-Gabitzsch *et al.*[21] have made kinematically complete studies by detecting both the pion and proton with momenta and angles such that the invariant mass $M_{\pi p}$ was in the vicinity of the $\Delta(1232)$.

Proton spectra from the related processes

$$np \to pn\pi^0, \tag{2a}$$

$$np \to pp\pi^- \tag{2b}$$

have been reported from Saclay.[22] By comparing our results to Saclay's and making use of the isospin arguments and approximations in the next section, one is able to estimate the fraction of nonresonant production present in Eqs. (2a) and (2b). This estimate is also presented in Sec. V.

II. BACKGROUND (OPE DIAGRAMS AND ISOSPIN AMPLITUDES)

The dominant diagrams for the process in Eq. (1) are the OPE graphs in Figs. 1(a) to 1(d), where the FSI between the pion and a nucleon is contained implicitly in the B vertices. Because this FSI has such a prominent effect, it is convenient to utilize

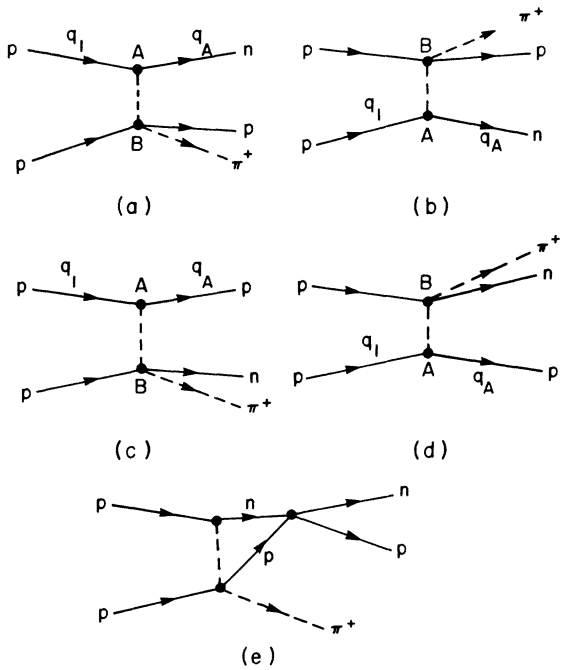

FIG. 1. The simplest OPE diagrams are shown in (a) through (d). Diagram (e) represents that in (a) modified by the *NN* FSI. Three other similar *NN* FSI diagrams correspond to those in (b) through (d). The top left line of each diagram represents the incident proton.

amplitudes which single out the isospin state of the πN system at the B vertices. The amplitude $A_{13}(p\pi)$, for example, refers to diagrams 1(a) and 1(b), where the second index 3 indicates that the πp isospin $I_{\pi p} = \frac{3}{2}$ and the first index, 1, indicates the initial-state I spin $I_{pp} = 1$. Diagrams 1(c) and 1(d) require both $I_{\pi n} = \frac{3}{2}$ and $I_{\pi n} = \frac{1}{2}$ amplitudes which are represented by $A_{13}(\pi n)$ and $A_{11}(\pi n)$, respectively. When np initial states are considered, the only additional amplitudes needed are all of the type A_{01}. The use of these amplitudes facilitates a comparison between processes (1) and (2), when the Clebsch-Gordan algebra is applied with the assumption of isospin invariance and with several other simplifications (see Appendix). From the Appendix the squared matrix element for process (1) is

$$\begin{aligned} |\langle np\pi^+|T|pp\rangle|^2 \cong{}& \tfrac{3}{4}|A_{13}(\pi p)|^2 + \tfrac{2}{3}\langle|A_{11}(\pi n)|^2\rangle \\ &+ \sqrt{2}\,\mathrm{Re}\langle A_{13}^*(\pi p)A_{11}(\pi n)\rangle \\ &+ \tfrac{1}{12}\langle|A_{13}(\pi n)|^2\rangle \\ &- (\tfrac{2}{9})^{1/2}\,\mathrm{Re}\langle A_{13}^*(\pi n)A_{11}(\pi n)\rangle \\ &- \tfrac{1}{2}\,\mathrm{Re}\langle A_{13}^*(\pi p)A_{13}(\pi n)\rangle\,. \end{aligned} \tag{3}$$

The angular brackets on the right-hand side indicate an average over the values of invariant mass of the πn system, $M_{\pi n}$, since this quantity is not unique for a specified neutron momentum. For this reaction $A_{01}(\pi n)$, $A_{01}(\pi p)$, and $A_{11}(\pi p)$ are necessarily zero. For each diagram in Figs. 1(a) to 1(d) the virtual-pion 4-momentum squared is given by $t = (q_1 - q_A)^2$, where q_1 and q_A are different for each diagram. For 0° neutrons it can be shown, for neutron momenta greater than 650 MeV/c, that t is smallest for the graph in Fig. 1(a). Since it can also be shown that each diagram separately contributes approximately as $1/|t|$ this first graph through the amplitude $A_{13}(\pi p)$ tends to overwhelm the others. Therefore, the fourth and fifth terms in Eq. (3) are expected to be negligible, especially in view of the smallness of their numerical coefficients. The last term is also expected to be negligible, because the phase of $A_{13}(\pi p)$ is essentially constant while that of $A_{13}(\pi n)$ is changing rapidly while being averaged over $M_{\pi n}$ near $M_{\pi n} = 1230$ MeV/c^2. The second and third terms are thus some measure of the nonresonant contribution to pion production in pp collisions, but since the neutrons are at 0° and high momentum transfer is involved in $A_{11}(\pi n)$, this contribution will be considerably diminished. Thus, the first term is dominant, and we can write for the squared matrix element, to a good approximation,

$$|\langle np\pi^+|T|pp\rangle|^2 \approx \tfrac{3}{4}|A_{13}(\pi p)|^2\,. \tag{3'}$$

However, it should be noted that the above inter-

ference terms are not necessarily negligible when integration is carried out over large regions of both nucleon momenta as is done by Guzhavin *et al.*[13] Since they neglected the interference between $A_{13}(\pi p)$ and $A_{13}(\pi n)$, their conclusion that $|A_{11}|^2/|A_{13}|^2 = 0.4$ is questionable.

The potential importance of these interference terms for total cross-section calculations is illustrated by a comparison of two theoretical predictions for the ratio $R = \sigma(pp \to \pi^+)/\sigma(pp \to \pi^0)$. The Mandelstam model,[1] which includes the interference terms, predicts $R = 3.9$ at 660 MeV on the assumption that $A_{11} = 0$, while the prediction with no interference[8] is $R = 5.0$. Since the experimental result[13,16] 650 MeV is $R \approx 3.0$, either the interference is important or A_{11} is not negligible, or both are true.

When the proton is detected at 0° in process (2a), arguments similar to those given above for the smallness of $A_{13}(\pi n)$ suggest that terms containing $A_{13}(\pi p)$, $A_{11}(\pi p)$, and $A_{01}(\pi p)$ can also be neglected, which is equivalent to neglecting the diagrams in Figs. 1(c) and 1(d) for the process in Eq. (1), and the summed squared matrix element in this case (see Appendix) becomes

$$|\langle pn\pi^0|T|pn\rangle|^2 + |\langle pp\pi^-|T|pn\rangle|^2 = \tfrac{1}{4}|A_{13}(\pi n)|^2 + \tfrac{1}{4}|A_{11}(\pi n) + A_{01}(\pi n)|^2 , \tag{4}$$

provided one assumes that $A_{ij}(\pi p)$ for (2b) equals $A_{ij}(\pi n)$ for (2a). If it is assumed that A_{11} and A_{01} are much smaller than A_{13} and can safely be neglected, the ratio of 0° cross sections for processes (1) and (2), from Eqs. (3′) and (4), is

$$\frac{\sigma(\theta_n = 0^\circ,\ pp \to np\pi^+)}{\sigma(\theta_p = 0^\circ,\ np \to pn\pi^0) + \sigma(\theta_p = 0^\circ,\ np \to pp\pi^-)} \cong 3.0 . \tag{5}$$

The neglect of Coulomb effects and the $\pi^0 - \pi^+$ mass difference in Eqs. (3) to (5) are approximations which introduce additional uncertainties of ~5%. Larger departures of the cross-section ratio of Eq. (5) from the value 3.0 provide a measure of the importance of the nonresonant amplitudes A_{11} and A_{01}.

Previous experimental evidence[10,13,16–19] for significant contributions from these amplitudes is weakened by the statistical inadequacy and inconsistency of the data. For example, it can be shown that, if the only nonzero amplitude is A_{13}, the shapes of the spectra for $pp \to \pi^0$ and $np \to \pi^\pm$ will be the same. While the shape of the π^0 spectrum of Bayukov and Tyapkin[20] at ~660 MeV is consistent with the $\pi^\pm$ spectral shape of Dzelepov *et al.*[17] at ~600 MeV, other π^0 data in the same energy region[12,13] show a markedly different shape. It is anticipated that a comparison of the recent $\pi^\pm$ spectra at 800 MeV (see Ref. 23) with the π^0 spectrum at 735 MeV (see Ref. 24) would help resolve this confusion. Meanwhile, the ratio of the cross sections in Eq. (5) can now be computed by making use of the recent Saclay[22] results and thereby yield a direct measure of the importance of A_{11} and A_{01}. This comparison is made in Sec. V.

III. EXPERIMENTAL APPARATUS AND DATA ACCUMULATION PROCEDURES

The LAMPF proton beam was focused onto a liquid-hydrogen (LH_2) production target (see Fig. 2) and the charged component of the transmitted beam was deflected magnetically by 60° and transported to a beam dump. Neutrons were transmitted through a collimator channel at 0° and studied by use of a multiwire proportional chamber (MWPC) spectrometer to detect the protons from charge-exchange scattering in an LH_2 radiator.

The proton-beam current was measured by integrating the output of a toroidal current monitor[25] through which the beam passed, upstream of the production target. This device was somewhat un-

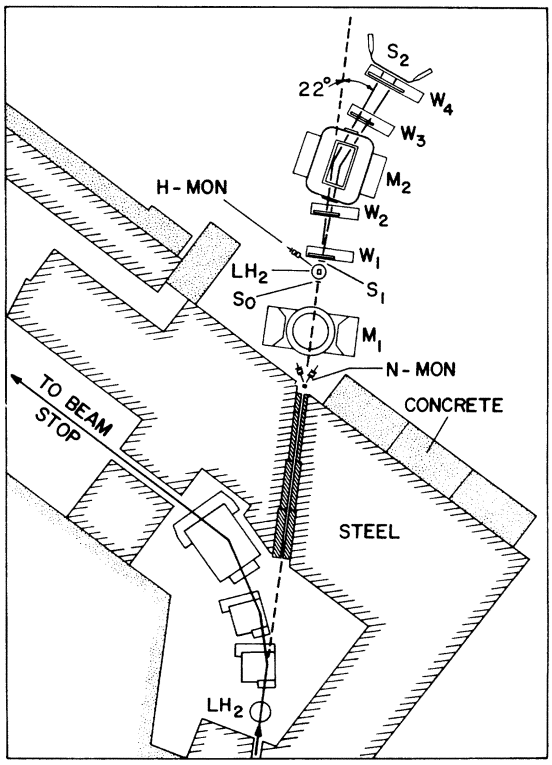

FIG. 2. Experimental arrangement of the proton beam and spectrometer. The dashed line represents the neutrons produced in the LH_2 production target inside the shielding wall.

stable during this experiment, and the overall accuracy was ±10%, which was one of the major uncertainties in the absolute normalization of the cross sections. The beam was focused and centered on the entrance window of the production target with the aid of wire-scanning devices. The size of the beam spot was ~0.5 × 1.0 cm, which was much smaller than the window opening of 3.2 × 15.2 cm. Both entrance and exit windows were made of aluminum of 0.013-cm thickness.

The production target contained ~10 liters of liquid hydrogen under forced convection in a closed loop. The fluid was cooled in a counter-current heat exchanger by gaseous helium from a Cryovac helium refrigerator of 250-watt cooling capacity at 20 °K. The pressure and temperature of the LH_2 were determined with hydrogen vapor bulbs within the loop. Thermal insulation was provided by the beam-line vacuum and by a radiation shield maintained at 77 °K. The areal density of hydrogen seen by the beam was 0.77 g/cm^2, which, at 800 MeV, produced an average proton energy loss of ~4.2 MeV (in addition to the 0.07-MeV energy loss in the entrance window). The target could be lifted out of the beam and replaced by a dummy in order to determine the contribution not coming from hydrogen.

The collimator was a hole of diameter 2.54 cm and length 366 cm through the steel and concrete shielding wall which enclosed the production target. It was constructed from a 155-mm gun barrel filled with machined steel inserts. The collimator axis was aligned to the incident-beam direction within 0.4 mrad. The downstream end of the collimator was 1095 cm from the LH_2 target, which gives a nominal collimation solid angle of 9.1×10^{-6} sr (i.e., a half angle of 0.1°).

Contaminant charged particles were swept from the neutron beam with magnet M_1 (see Fig. 2), and any residual contamination was eliminated by use of a veto scintillator S_0 in front of the LH_2 radiator. The neutron beam was monitored at the collimator exit by detecting charged particles from a polyethylene radiator of thickness 2.54 cm with a pair of range telescopes (called the N-Mon) symmetrically placed at left and right scattering angles of 25°. An additional monitor was provided by another range telescope which detected protons scattered at 45° from the LH_2 radiator.

The LH_2 radiator consisted of about one liter of liquid hydrogen contained in a Mylar flask of wall thickness 0.013 cm. The liquid was cooled by a 10-watt, two-stage helium-expansion refrigerator The liquid could be forced from the flask into a reservoir by hydrogen vapor in order to determine background contributions from the container. Thermal isolation was provided by a vacuum, by a radiation shield maintained by liquid N_2 at an intermediate temperature, and by several layers of aluminized Mylar wrapped around the flask. A window in the vacuum enclosure covered by Mylar of 0.013-cm thickness permitted charged particles to escape from the target. The total thickness of Mylar traversed by such particles was ~0.026 cm. The areal density of LH_2 in the beam direction was 0.94 g/cm^2.

The MWPC spectrometer[26] consisted of a large dipole magnet (M_2), four horizontal-vertical pairs of MWPC's ($W_1 - W_4$), and two thin scintillators (S_1 and S_2). An event was accepted for processing when signals from S_1, S_2, and at least three out of four of both horizontal and vertical MWPC's were in coincidence and not vetoed by a signal from S_0. On acceptance of the event, an inhibit signal was generated to prevent changes in the MWPC and analog signal data while they were being processed. This inhibit signal generated a gate whose length was determined by the time needed to read in the analog signals and the MWPC data. The deadtime of the system was measured by a comparison of the gated N-Mon counts to the ungated counts. This deadtime was about 13% for these data which were accumulated at a rate of ~65 events/sec. At this rate the deadtime effects caused by the veto from S_0 were well under 1% and were neglected.

The timing between the signals from S_1 and S_2 gave the time of flight t_{12} of the particle through the spectrometer. The timing t_r of the S_1 signal relative to the accelerator rf cycle provided a measure of the neutron time of flight between the production target and S_1 when the beam was run in a special mode (chopped) whereby only one in eight micropulses contained protons. The signals from the MWPC's were encoded so as to identify the wires from which the signals had come. When this information had been transferred to a fast intermediate buffer called the scratch pad memory (SPM)[26] and the analog signals for t_{12}, t_r, and the pulse heights from S_1, S_{2l}, and S_{2r} (scintillator S_2 was viewed from both edges) had been sent via CAMAC to a micro-programmed branch driver (MBD),[27] the inhibit was lifted. The data were transferred from the MBD to a PDP 11/20 computer during the 7.8-msec off-period between beam macropulses.

The MWPC's provided a determination of the particle trajectories before and after deflection by the magnet. Since the field of the magnet is well known, having been mapped on a three-dimensional grid of ~80 000 points for each of four different magnet currents, the path of the particle through the spectrometer could be reconstructed and the momentum deduced even if signals from one vertical and one horizontal wire plane were

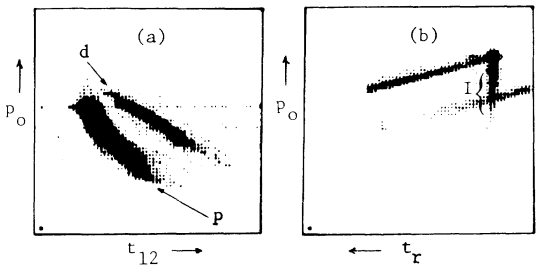

FIG. 3. On-line display of 2-parameter plots. (a) P_0 (actually the reciprocal of the horizontal bend angle) vs TOF between S_1 and S_2. (b) P_0 vs TOF between production target and S_1 making use of the *RF* pulse structure with "chopped" beam. The inelastic events are indicated by I.

absent. The sense-wire spacing of the MWPC's was 2.0 mm, and the separation between W_1 and W_2 and between W_3 and W_4 was 100 cm. This permitted determination of the deflection with an accuracy of ~2 mrad on the average. Thus, a typical deflection of 22° (~380 mrad) was determined with an accuracy of ~0.5%, which determined the momentum to that accuracy. The resolution of the spectrometer was degraded somewhat by the effects of multiple scattering and energy loss. Most of this came from the LH_2 radiator and S_1 (thickness = 0.079 cm), although W_1, W_2, and W_3 (effective thickness $\cong$ 63 mg/cm^2) also contributed. The contribution from the spaces between the MWPC's was minimized by filling these spaces with helium contained by plastic bags. In the end, the overall resolution of the spectrometer was around 1%.

The on-line data acquisition program[28] wrote all data for each event on magnetic tape for use in later off-line analysis as well as providing live display of a variety of histograms and two-parameter plots of a subset of the data (i.e., those events in which one "hit" wire was registered in each wire plane). Two examples of particular interest and importance are shown in Figs. 3(a) and 3(b). They are plots of the approximate momentum p_0 (estimated from the angle of deflection) vs t_{12}, and t_r, respectively. Figure 3(a) illustrates how particle identification was perceived on-line and Fig. 3(b) shows how it could be determined whether a recoil of low momentum came from elastic scattering of a low-momentum neutron or from an inelastic reaction of a high-momentum neutron in the radiator. The off-line program discussed in Sec. III was used to refine these plots and thereby extract the required separation.

The data were taken during different time periods at nominal proton-beam energies of 650, 766, and 800 MeV. The 766- and 800-MeV data were taken several months apart and their comparison provides some check of the stability and internal consistency of the measurements. In order to obtain the momentum spectrum over a wide region, data were obtained with five different spectrometer magnet currents. The extent of overlap and degree of internal consistency for some of the 766-MeV data are illustrated in Fig. 4.

In order to eliminate the background contribution coming from the container walls of the production target and the radiator, data were obtained with

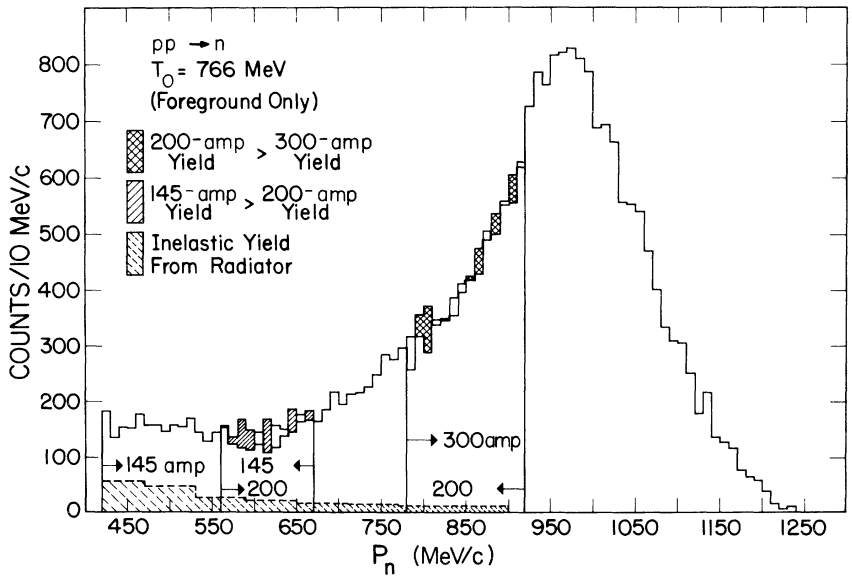

FIG. 4. Data of a raw momentum spectrum showing the overlap for three different settings of the current in M_2. The effect of pion production in the radiator is shown as the inelastic yield from radiator and has yet to be subtracted here.

the radiator emptied and the filled production target in place, with a full radiator and the dummy production target in place, as well as with both radiator and production target filled and in place. The background yields were both less than 10% of the foreground yield and were independently subtracted from it. (The error caused by the double subtraction of the contribution due to interactions in the walls of both containers was less than 1% and could be neglected.)

The background for 800 MeV due to double pion production was estimated to be less than 2% (see Ref. 10) except in the region 460 MeV/$c < P_n < 860$ MeV/c; there it was estimated to be as high as 4% based on the observed π^- production in 735-MeV pp collisions.[11] Since the statistical precision in this spectral region for both 766 and 800 MeV is only 10%, the background from double pion production was neglected.

Normally the accelerator provides beam in micropulses of less than $\frac{1}{4}$-nsec duration and 5-nsec separation, and most of the data were obtained with beam of such time structure. The utility of such structure in neutron TOF measurements is limited by the inability to determine which micropulse produced the neutron. Thus, TOF cannot be used to determine whether or not a low-energy recoil proton is to be attributed to an inelastic reaction in the radiator. Such reactions contribute a background which must be removed in determination of the neutron spectrum. A special set of runs using the chopped mode was made to determine an empirical correction for this radiator inelasticity. In these runs, aluminum was used as a production target in a deliberate attempt to increase the yield of neutrons of lower momentum,[29] and the accelerator was operated in the optional chopped mode in which the micropulse separation was increased to 40 ns, making possible a crude but unambiguous determination of the neutron momentum by TOF measurement with a flight path of 11 m. The inelastic contribution for each region of neutron momentum was then determined from the spectrum of recoil protons seen in the spectrometer, where the elastic and inelastic protons were clearly separated, as shown by I in Fig. 3(b). However, the data so obtained were of limited statistical accuracy, but the corrections were large only for the lowest momentum region (see Fig. 4) and will be improved by obtaining more data of this type in the future.

IV. DATA ANALYSIS

The data were analyzed off-line in two stages, represented by different computer programs TEWA (see Ref. 30) and KIOWA (see Ref. 31). The primary functions of TEWA were to analyze each event by determining the value of particle momentum p most compatible with the MWPC information and to record this and other important information on the event (e.g., analog signal values, calculated orbit parameters, χ^2 value for the fit, origin of the event in the radiator, diagnostic information) in a standard format on an intermediate tape. It began by decoding the MWPC information to determine the coordinates of the wire-plane hits; if two or more contiguous wires in one plane were hit (a cluster), it calculated the position of the centroid for the group. If one x and/or y coordinate were missing, it would reconstruct the missing coordinate(s) on the assumption that the incoming and outgoing trajectories intersect near the mid-plane of the magnet. From the coordinates it would calculate the angle of deflection, and from this a fairly accurate estimate p_0 of the momentum could be made. The path of a particle of momentum p_0 was determined by numerical integration through the mapped field of the magnet. Finally, an expression for χ^2 involving the measured and calculated incoming and outgoing orbit parameters and the momentum was minimized to determine optimum values for these variables. The process could be reiterated, but it was found by experience that one iteration usually gave momentum values within 0.5% of the final values.

In cases where there were multiple clusters, two options were available. In the first, all possible trajectories for the event were considered and the two with the best χ^2 values were kept. In the second, if only one x and/or y coordinate was multivalued, it was treated as if it were missing; more complex events were rejected. The different treatments led to results which differed especially at low momenta. The first option was used on a selected subset of data to establish correction factors that were applied to the rest of the data which were handled with the second option.

The program KIOWA was used to sort the events on the intermediate tape according to particle identity, momentum p, times of flight t_{12} and t_r, scattering angles θ and ϕ, etc. It also was adapted to make corrections and background subtractions, merge data, and calculate cross sections.

One of the preliminary uses of KIOWA was in an empirical determination of the geometric acceptance of the spectrometer, which was limited vertically by the magnet poles and horizontally by the edges of the MWPC's. However, because of the finite beam size, the origin of the charge-exchange scattering varied from event to event and the geometric limitations did not map into a sharply defined region of acceptance for θ and ϕ, although there was a "safe" θ-ϕ region within

which there was negligible probability that the particle could strike a magnet pole or miss one of the MWPC's. For our experimental geometry and beam size, the vertical extent of the safe region was given by $\sin\theta \sin\phi \leq 0.02$. Imposition of this restriction limits the azimuthal angular acceptance to the fraction $\epsilon = (2/\pi) \arcsin (0.02/\sin\theta)$ when $\sin\theta > 0.02$, but eliminated uncertainty about the eclipsing due to the magnet poles.

The horizontal limits to the safe region, for both left (θ_L) and right (θ_R) scattered particles, were determined by the edges of the wire chambers. These limits, for a given spectrometer magnet current, are a function of particle momentum and were measured by examination of plots of θ vs wire position for different momentum bands. It was found that constant θ_L and θ_R limits of 0.04 rad could be used over a wide momentum range ($\Delta p/p = 0.52$) for a given magnet current without loss of particles. This acceptance region enabled direct comparison of counts obtained in overlapping momentum intervals for different magnet currents as well as simplifying the correction made necessary by the variation in the *np* charge-exchange cross section.

The recoil-proton spectra were converted to neutron spectra by dividing out the momentum dependence of the *np* charge-exchange scattering (*np* CEX) differential cross section. This was done by consideration of $\Delta\sigma_{np}(p_i)$, the cross section by which neutrons of momentum p_i were converted into protons which entered the spectrometer acceptance region. We calculated $\Delta\sigma_{np}$ from a subset[32] of the various sets of *np* CEX data that exists in the momentum range of interest. The relation used was

$$\Delta\sigma_{np}(p_i) = 2\pi \int_0^{0.04} \epsilon(\theta)(d\sigma(\theta, p_i)/d\Omega)\sin\theta \, d\theta \,,$$

where $d\sigma/d\Omega$ represents the laboratory *np* CEX differential cross section, θ is the proton polar angle, and $\epsilon(\theta)$ is the geometrical efficiency which at given θ represents the fraction of azimuthal angle allowed by the magnet pole faces. A straight line[29] was chosen to represent $\Delta\sigma_{np}$ as a function of momentum. This line passed through the results of the absolute experiments[32] of Scanlon *et al.* at 99 MeV, Kazarinov *et al.* at 200 MeV, and recent results of our group at 647 MeV. The straight line is given by

$$\Delta\sigma_{np}(p) = (-2.19 \times 10^{-5} p + 0.174) \text{ mb} \,,$$

where p is the momentum in MeV/c. The final absolute double differential cross sections were then obtained by normalizing with respect to the incident proton beam intensity, the collimator solid angle, and the areal densities of production and scattering targets.

The error in the absolute normalization was determined essentially from the uncertainty in the *np* charge-exchange cross section over the energy region 75 to 530 MeV,[29,32] and the accuracy of the proton-beam-current monitor mentioned in Sec. III. These systematic errors and several others were estimated as follows.

np charge exchange	±10%
current monitor	±10%
production target density	±2%
radiator density	±2%
collimator solid angle	±2%
spectrometer efficiency	±1%

These sources of systematic error combine to give approximately 15% error for the absolute normalization.

V. RESULTS AND CONCLUSIONS

The 0° neutron momentum spectra in the laboratory from process (1) are shown in Fig. 5 along with the results of the modified SGG calculation.[5] From the diagram in Fig. 1(a) one might expect these spectra to peak for $M_{\pi p} \approx 1232$ MeV/c^2, but the broad peak in each case centers at $M_{\pi p} \approx 1200$ MeV/c^2. These spectral peaks are shifted partly because the Δ(1232) resonance actually produces

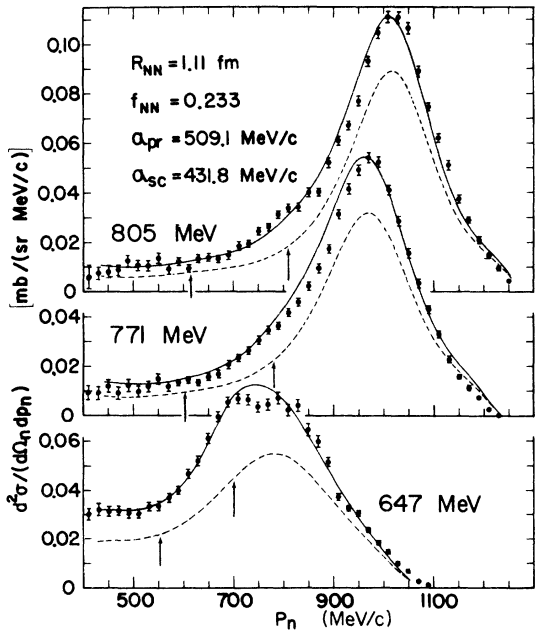

FIG. 5. The three neutron momentum spectra at 0°. The left-hand arrow in each case indicates the neutron laboratory momentum, P_n, for which the neutron is stationary in the c.m. system while the right-hand arrow locates that value of P_n where the two final state nucleons are expected to have the largest interaction.

TABLE I. Summary of c.m. spectra.

$T_{\text{inc}}^{\text{lab}}$ (MeV)	$\left(\frac{d^2\sigma}{dp_n^* d\Omega^*}\right)_{\text{peak}}$ [a] [mb/(sr MeV/c)]	$\left(\int dp_n^* \frac{d\sigma}{dp_n^* d\Omega^*}\right)$ [b] (mb/sr)	$(M_{\pi p})$ peak (MeV/c^2)	$\Delta M_{\pi p}$ FWHM (MeV/c^2)
647	0.0072±0.0002	1.40±0.20	1188±5	70±5
771	0.013 ±0.0003	2.15±0.31	1199±5	82±5
805	0.015 ±0.0003	2.43±0.36	1200±5	75±5

[a] Statistical error only is quoted here.

[b] Normalization error only is quoted here and the integral is over only those neutrons in the forward hemisphere in the c.m. system.

a peak at 1225 MeV in the $\pi^+ p$ total cross section, which enters as a phenomenological factor in the pion production cross section. The rest of the shift is due to phase-space factors and the propagators associated with OPE.[2,5] In Table I the peak positions and widths, in terms of $M_{\pi p}$, are tabulated along with the integrated and the peak cross sections in the center-of-mass (c.m.) system.

The results of the modified SGG calculation are represented by the solid and dashed curves in Fig. 5. Diagrams such as that shown in Fig. 1(e) have been included in the full calculation (solid line) but are left out for the dashed curves. Four parameters are used: $\alpha_{\pi\pi}$ and α_{sc} account for the off-shell effects of the exchanged pion at the production (A) and scattering vertices (B) in Fig. 1(a) to 1(d); f_{NN} is used to scale the effects of the NN rescattering-type diagrams [Fig. 1(e)] and R_{NN} is a length characteristic of the average separation of the two nucleons in the final state. The scattering vertices are handled phenomenologically using a set of πp phase shifts including only S and P waves. The parameter values were derived by a fit to the 805-MeV data by the method of steepest descent. The 1% uncertainty in the beam energy permits some shifting in the incident energy in order to optimize the fit. The nominal incident energies were 647, 764, and 798 MeV, but the fit was much improved by raising the last two energies by 7 MeV, well within the 1% tolerance. However, note that the 34-MeV difference between these two energies is preserved, as would be expected in view of the modular technique used at LAMPF to change the beam energy. It is both striking and encouraging that the parameters determined from fits to the 805-MeV data do so well in predicting the 647- and 771-MeV results.

Clearly, the effect of the $\Delta(1232)$ resonance is the dominant feature, particularly at 771 and 805 MeV, although there is a definite need for substantial contributions from the rescattering diagrams such as Fig. 1(e), especially in the 647-MeV spectrum. Since the Mandelstam model[1] incorporates NN FSI explicitly and works successfully up to 650 MeV, it is not surprising to find that the rescattering diagrams make contributions comparable to those of the OPE diagrams at 647 MeV.

The data in Fig. 5 are plotted in bins of 20 MeV/c, whereas the spectrometer resolution is better than 15 MeV/c. Hence, the extent of the deviations from the theory are larger than the spectrometer resolution and they seem to be statistically significant. These deviations are not surprising in view of the approximations in the model of SGG.

Since the process in Eq. (1) is symmetric in the (c.m.) system of the two incident protons, it is informative to present the data for 805 MeV in this c.m. system, as is done in Fig. 6. From this plot it is evident that the lower limit of the spectrometer is around 400 MeV/c ($\beta p = 157$ MeV/c for multiple scattering); above this momentum the data show the symmetry that is expected, which demonstrates the internal consistency of our measurements.

A comparison between processes (1) and (2) is made in Fig. 7, where the Saclay data[22] and the

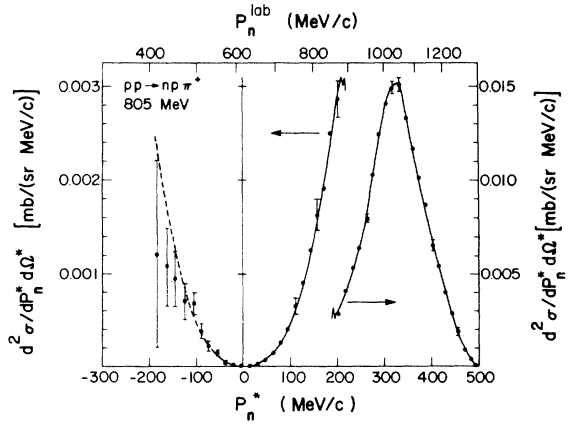

FIG. 6. The 805-MeV neutron momentum spectrum in the c.m. system. The dashed line is a reflection of the solid line which is drawn to guide the eye.

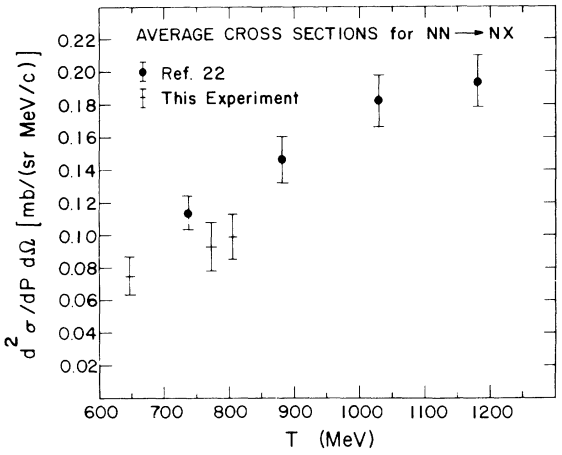

FIG. 7. A comparison to the Saclay results of Ref. 22 which are multiplied by 3.0. The indicated errors represent normalization uncertainty, 10% in the case of Ref. 22 and 15% in the present experiment.

present results are plotted as cross sections averaged over a 150-MeV/c bin centered at the pion production peak. The Saclay averaged cross sections are multiplied by 3.0 to account for the ratio in Eq. (5). From this plot at around 800 MeV it is seen that the ratio $(pp \to np\pi^+)/(np \to pX)$ is 2.34 ± 0.42 instead of 3.0. From Eqs. (3′) and (4) it can then be inferred that

$$\frac{|A_{11}(\pi n)+A_{01}(\pi n)|^2}{|A_{13}(\pi p)|^2} = 0.28 + 0.28/-0.20 .$$

While this result is of low precision it is not inconsistent with the conclusion of Ref. 13 that $|A_{11}|^2/|A_{13}|^2 \approx 0.4$.

The measurements presented here have allowed for a detailed study of process (1) in an energy region where the underlying physical mechanisms for pion production are changing quite rapidly. The data presented here should be supplemented by comparable data at other angles in order to motivate further development of pion production theories. It is anticipated that such data will be forthcoming in the near future.[21] Should the SGG calculation be found to fit the data as well as it does here for both higher and lower energies and for angles other than 0°, without changing the parameter values, then there will finally exist a successful phenomenology for single-pion production in nucleon-nucleon collisions over an extended energy region.

ACKNOWLEDGMENTS

We thank the LAMPF operations group and all the personnel led by Dr. Don Hagerman and Dr. Lew Agnew, who contributed to the success of this experiment. Those of us who have been visitors to the Los Alamos Scientific Laboratory (LASL) would also like to express our appreciation for the hospitality granted us. Jan Boissevain, who helped in many technical areas, and the various support groups at LASL which are represented by Stretch Fretwell, Anne Niethammer, and Dr. Ken Williamson are also deserving of much credit in this effort. Dr. R. Slansky, Dr. J. Stephenson, Dr. W. Gibbs, and Dr. B. Gibson have been extremely helpful in discussions. We are also grateful to them for providing us with the SGG code and to Dr. H. Bryant for his many contributions.

APPENDIX

If we write isotopic-spin states as $|I,I_z\rangle$ or $\langle I,I_z|$ the initial state for the process of Eq. (1) is

$$|pp\rangle = |1,1\rangle \tag{A1}$$

and the final state can be written either as

$$\langle np\pi^+|_n = \langle n|\langle \pi^+ p| = \langle \tfrac{1}{2}, -\tfrac{1}{2}|\langle \tfrac{3}{2}, \tfrac{3}{2}| \tag{A2a}$$

[corresponding to the graphs in Figs. 1(a) and 1(b)], or as

$$\langle np\pi^+|_p = \langle p|\langle \pi^+ n| = \langle \tfrac{1}{2},\tfrac{1}{2}|[(\tfrac{1}{3})^{1/2}\langle \tfrac{3}{2},\tfrac{1}{2}| + (\tfrac{2}{3})^{1/2}\langle \tfrac{1}{2},\tfrac{1}{2}|] \tag{A2b}$$

[corresponding to the graphs in Figs. 1(c) and 1(d)]. From Clebsch-Gordan algebra each of these forms of the final state can be expressed generally in terms of total isospin states as follows:

$$\langle np\pi^+|_n = (\tfrac{1}{4})^{1/2}\langle 2,1|_{3/2} + (\tfrac{3}{4})^{1/2}\langle 1,1|_{3/2} , \tag{A3a}$$

$$\langle np\pi^+|_p = (\tfrac{1}{4})^{1/2}\langle 2,1|_{3/2} - (\tfrac{1}{12})^{1/2}\langle 1,1|_{3/2} + (\tfrac{2}{3})^{1/2}\langle 1,1|_{1/2} . \tag{A3b}$$

The fractional subscripts serve to distinguish the total isospin states in terms of the πN isospin system they contain.

The amplitudes mentioned in Sec. II, which relate to each of the diagrams in Figs. 1(a) to 1(d), can now be defined as

$$A_{13}(\pi p) \equiv \langle 1,1|_{3/2} T(\pi p)|1,1\rangle \tag{A4a}$$

for the graphs of Figs. 1(a) and 1(b), and

$$A_{13}(\pi n) \equiv \langle 1,1|_{3/2} T(\pi n)|1,1\rangle ,$$
$$A_{11}(\pi n) \equiv \langle 1,1|_{1/2} T(\pi n)|1,1\rangle , \tag{A4b}$$
$$A_{01}(\pi n) \equiv \langle 0,0|_{1/2} T(\pi n)|0,0\rangle$$

for the graphs of Figs. 1(c) and 1(d). As noted previously, the arguments of A_{ij} and T serve to distinguish which set of diagrams each of the amplitudes represents. If isospin invariance is

invoked and Eqs. (A3) and (A4) are combined, the total matrix element is found to be

$$\langle np\pi^+|T|pp\rangle = (\tfrac{3}{4})^{1/2}A_{13}(\pi p) - (\tfrac{1}{12})^{1/2}A_{13}(\pi n) + (\tfrac{2}{3})^{1/2}A_{11}(\pi n)\,, \quad \text{(A5)}$$

which leads directly to Eq. (3).

The final states for the process of Eq. (2a) can be written either as

$$\langle pn\pi^0|_p = \langle p|\langle n\pi^0| = \langle \tfrac{1}{2},\tfrac{1}{2}|[(\tfrac{2}{3})^{1/2}\langle \tfrac{3}{2},-\tfrac{1}{2}| + (\tfrac{1}{3})^{1/2}\langle \tfrac{1}{2},-\tfrac{1}{2}|]\,, \quad \text{(A6a)}$$

or as

$$\langle pn\pi^0|_n = \langle n|\langle p\pi^0| = \langle \tfrac{1}{2},-\tfrac{1}{2}|[(\tfrac{2}{3})^{1/2}\langle \tfrac{3}{2},\tfrac{1}{2}| - (\tfrac{1}{3})^{1/2}\langle \tfrac{1}{2},\tfrac{1}{2}|]\,, \quad \text{(A6b)}$$

which leads to

$$\langle pn\pi^0|_p = (\tfrac{1}{3})^{1/2}\langle 2,0|_{3/2} - (\tfrac{1}{3})^{1/2}\langle 1,0|_{3/2} + (\tfrac{1}{6})^{1/2}\langle 1,0|_{1/2} + (\tfrac{1}{6})^{1/2}\langle 0,0|_{1/2} \quad \text{(A7a)}$$

and

$$\langle pn\pi^0|_n = (\tfrac{1}{3})^{1/2}\langle 2,0|_{3/2} + (\tfrac{1}{3})^{1/2}\langle 1,0|_{3/2} - (\tfrac{1}{6})^{1/2}\langle 1,0|_{1/2} + (\tfrac{1}{6})^{1/2}\langle 0,0|_{1/2}\,. \quad \text{(A7b)}$$

As before, Eqs. (A6a) and (A6b) each relate to one set of diagrams. For the process in Eq. (2b) only one form of the final state is needed and gives

$$\langle pp\pi^-| = \langle p|\langle p\pi^-| = \langle \tfrac{1}{2},\tfrac{1}{2}|[(\tfrac{1}{3})^{1/2}\langle \tfrac{3}{2},-\tfrac{1}{2}| - (\tfrac{2}{3})^{1/2}\langle \tfrac{1}{2},-\tfrac{1}{2}|] \quad \text{(A8)}$$

to yield

$$\langle pp\pi^-| = (\tfrac{1}{6})^{1/2}\langle 2,0|_{3/2} - (\tfrac{1}{6})^{1/2}\langle 1,0|_{3/2} - (\tfrac{1}{3})^{1/2}\langle 1,0|_{1/2} - (\tfrac{1}{3})^{1/2}\langle 0,0|_{1/2}\,. \quad \text{(A9)}$$

The initial state for these latter two processes is

$$|pn\rangle = (\tfrac{1}{2})^{1/2}|1,0\rangle - (\tfrac{1}{2})^{1/2}|0,0\rangle\,,$$

which, when isospin invariance is invoked, gives for the process in Eq. (2a)

$$\langle np\pi^0|T|np\rangle = (\tfrac{1}{6})^{1/2}[A_{13}(\pi p) - A_{13}(\pi n)] - (\tfrac{1}{12})^{1/2}[A_{11}(\pi p) - A_{11}(\pi n)] - (\tfrac{1}{12})^{1/2}[A_{01}(\pi p) + A_{01}(\pi n)]\,. \quad \text{(A10)}$$

For (2b), when one assumes that $A_{ij}(\pi p)$ for (2b) equals $A_{ij}(\pi n)$ for (2a) one obtains

$$\langle pp\pi^-|T|pn\rangle = -(\tfrac{1}{12})^{1/2}A_{13}(\pi n) - (\tfrac{1}{6})^{1/2}A_{11}(\pi n) + (\tfrac{1}{6})^{1/2}A_{01}(\pi n)\,, \quad \text{(A11)}$$

where again we have neglected diagrams analogous to those in Figs. 1(c) and 1(d). Equation (4) then follows when Eqs. (A10) and (A11) are used with the approximations stipulated in Sec. II.

---

*Work performed under the auspices of the U. S. Energy Research and Development Administration.

†Present address: Los Alamos Scientific Laboratory, Los Alamos, New Mexico 87545.

‡Present address: University of Wyoming, c/o LAMPF Visitor Center, Los Alamos Scientific Laboratory, Los Alamos, New Mexico 87545.

§Present address: Science Applications, Inc., LaJolla, California 92037.

[1]S. Mandelstam, Proc. R. Soc. London A244, 491 (1958).

[2]E. Ferrari and F. Selleri, Nuovo Cimento 27, 1450 (1963).

[3]S. J. Lindenbaum and R. M. Sternheimer, Phys. Rev. 105, 1874 (1957).

[4]D. Drechsel and H. J. Weber, Nucl. Phys. B25, 159 (1970).

[5]W. R. Gibbs, B. F. Gibson, and G. J. Stephenson, Jr., contribution to the VI International Conference on High Energy Physics and Nuclear Structure, Santa Fe, 1975 (unpublished); R. C. Slansky, G. J. Stephenson, R. Gibbs, and B. F. Gibson, Bull. of APS, Ser. II 20, 83 (1975).

[6]L. I. Lapidus, Zh. Eksp. Teor. Fiz. 31, 865 (1956) [Sov. Phys.—JETP 4, 740 (1957)].

[7]K. C. Marish and L. M. Soloko, Zh. Eksp. Teor. Fiz. 40, 605 (1961) [Sov. Phys.—JETP 13, 423 (1961)].

[8]D. C. Peaslee, Phys. Rev. 94, 1085 (1954); 95, 1580 (1954).

[9]R. J. Eden, *High Energy Collisions of Elementary Particles* (Cambridge Univ. Press, Cambridge, 1967), p. 262.

[10]J. G. Rushbrooke, D. V. Bugg, A. J. Oxley, J. A. Zoll, M. Jobes, J. Kinson, L. Riddiford, and B. Tallini, Nuovo Cimento 33, 1509 (1964).

[11]D. R. F. Cochran, P. N. Dean, P. A. M. Gram, E. A. Knapp, E. R. Martin, D. E. Nagle, R. B. Perkins, W. J. Shlaer, H. A. Thiessen, and E. D. Theriot, Phys. Rev. D 6, 3085 (1972).

[12]B. Baldoni, S. Focardi, H. Hromadnik, L. Monari, F. Saporetti, S. Femino, F. Mezzanares, E. Bertolini, and G. Gialanella, Nuovo Cimento 26, 1376 (1962).

[13]V. M. Guzhavin, G. K. Kliger, V. Z. Kolganer, A. V. Lebedev, K. S. Marish, Yu. D. Prokoshkin, V. T. Smolyankin, A. P. Sokolov, L. M. Soroko, and Ts'Ui Wa-ch'uang, Zh. Eksp. Teor. Fiz. 46, 1245 (1964) [Sov. Phys.—JETP 19, 847 (1964)].

[14]D. V. Bugg, A. J. Oxley, J. A. Zoll, J. G. Rushbrooke, V. E. Barnes, J. B. Kinson, W. P. Dodd, G. A. Doran, and L. Riddiford, Phys. Rev. 133, B1017 (1964); V. E. Barnes, D. V. Bugg, W. P. Dodd, J. B. Kinson, and L. Riddiford, Phys. Rev. Lett. 7, 288 (1961).

[15]A. H. Rosenfeld, Phys. Rev. 96, 130 (1954); A. G. Meshkovskii, Ia. Ia. Shalamov, and V. A. Shebanov, Zh. Eksp. Teor. Fiz. 35, 64 (1958) [Sov. Phys.—JETP

8, 46 (1959)].
[16]Yu. D. Prokoshkin and A. A. Tyapkin, Zh. Eksp. Teor. Fiz. 32, 750 (1957) [Sov. Phys.—JETP 5, 618 (1957)].
[17]V. P. Dzhelepov, V. S. Kiselev, K. O. Oganesyan, and V. B. Flyagin, Zh. Eksp. Teor. Fiz. 50, 1491 (1966) [Sov. Phys.—JETP 23, 993 (1966)].
[18]Yu. M. Kazarinov and Yu. N. Simonov, Yad. Fiz. 4, 139 (1966) [Sov. J. Nucl. Phys. 4, 100 (1967)].
[19]A. F. Dunaitsev and Yu. D. Prokoshkin, Zh. Eksp. Teor. Fiz. 38, 747 (1960) [Sov. Phys.—JETP 11, 540 (1960)].
[20]Yu. D. Bayukov and A. A. Tyapkin, Zh. Eskp. Teor. Fiz. 32, 953 (1957) [Sov. Phys.—JETP 5, 779 (1957)].
[21]J. Pratt, R. Bentley, H. Bryant, R. Carlini, C. Cassapakis, B. Dieterle, C. Leavitt, T. Rupp, and D. Wolfe, contribution to the VI International Conference on High Energy Physics and Nuclear Structure, Sante Fe, 1975 (unpublished); J. Hudomalj-Gabitzsch, T. Witten, N. D. Gabitzsch, G. S. Mutchler, T. Williams, J. Clement, J. C. Phillips, E. Hungerford, L. Y. Lee, M. Warneke, B. M. Mayes, and J. C. Allred, *ibid.* 1975 (unpublished).
[22]G. Bizard, F. Bonthonneau, J. L. Laville, F. Lefebvres, J. C. Malherbe, R. Regimbart, J. Duflo, and F. Plouin, contribution to the VI International Conference on High Energy Physics and Nuclear Structure, Santa Fe, 1975 (unpublished) and unpublished work.
[23]D. W. Wolfe, C. Cassapakis, B. D. Dieterle, C. P. Leavitt, W. R. Thomas, G. Glass, M. Jain, L. C. Northcliffe, B. E. Bonner, and J. E. Simmons, contribution to the VII International Conference on Few Body Problems in Nuclear and Particle Physics, Delhi (unpublished).
[24]R. J. Cence, D. L. Lind, G. D. Mead, and B. J. Moyer, Phys. Rev. 131, 2713 (1963).
[25]P. J. Tallerico, Los Alamos Scientific Laboratory Report No. LA-UR-900, 1974 (unpublished).
[26]D. W. Werren, D. Brown, L. M. Fox, C. Pacheco, C. W. Bjork, B. E. Bonner, S. Cohen, F. D. Newcom, J. E. Simmons, H. C. Bryant, C. G. Cassapakis, B. D. Dieterle, D. M. Wolfe, and J. C. Hiebert, Los Alamos Scientific Laboratory Report No. LA-5396-MS, 1973 (unpublished); D. Brown, Nucl. Instrum. Meth. 117, 561 (1974).
[27]L. R. Biswell and R. E. Rajala, Los Alamos Scientific Laboratory Report No. LA-4916-MS, 1972 (unpublished).
[28]J. C. Hiebert and A. C. Niethammer, Los Alamos Scientific Laboratory Report No. LA-5609-MS, 1974 (unpublished).
[29]C. G. Cassapakis, H. C. Bryant, B. D. Dieterle, C. P. Leavitt, D. M. Wolfe, B. E. Bonner, J. E. Simmons, C. W. Bjork, P. J. Riley, M. L. Evans, G. Glass, J. C. Hiebert, M. Jain, R. A. Kenefick, L. C. Northcliffe, and D. W. Werren, Phys. Lett. 63B, 35 (1976).
[30]M. Jain, D. Werren, and H. Bryant (unpublished).
[31]M. Hutchinson, J. Friedman, and A. Rittenberg, UCRL Group A Programming Note No. p-171, 1973 (unpublished).
[32]J. P. Scanlon, G. H. Stafford, J. J. Thresher, P. H. Bowen, and A. Langsford, Nucl. Phys. 41, 401 (1963); A. J. Hartzler and R. T. Siegel, Phys. Rev. 95, 185 (1954); D. F. Measday, *ibid.* 142, 584 (1966); J. N. Palmieri and J. P. Wolfe, Phys. Rev. C 3, 144 (1971); Yu. M. Kazarinov and Yu. N. Simonov, Zh. Eksp. Teor. Fiz. 43, 35 (1962) [Sov. Phys.—JETP 16, 24 (1963)]; M. L. Evans, G. Glass, J. C. Hiebert, M. Jain, R. A. Kenefick, L. C. Northcliffe, B. E. Bonner, J. E. Simmons, C. W. Bjork, P. J. Riley, H. C. Bryant, C. G. Cassapakis, B. Dieterle, C. P. Leavitt, D. M. Wolfe, and D. W. Werren, Phys. Rev. Lett. 36, 497 (1976).